Surface wrinkling of freely-floating smectic bubbles

Patricia Pfeiffer[1]
Institute for Physics, Otto von Guericke University Magdeburg, Universitätsplatz 2, 39106 Magdeburg, Germany[a)]

Bubbles made of smectic liquid crystals (LC) can display buckling and wrinkling. These deformations are induced in the course of the relaxation of an elongated bubble towards a sphere. The bubbles are created through the collapse of a catenoid LC film. Two mechanisms leading to wrinkles are reported: (a) Compression of the smectic film by outer forces, and (b) Invagination of the bubble shortly after formation. The flow on the bubble surface is analyzed, providing insight into how the outer forces act on the bubble and induce local surface deformation. It is found that the orientation of the wrinkles depends on the direction of the acting force.
Additionally, the formation of small protrusions outside the film area (i. e., tubuli) is described.

I. INTRODUCTION

Wrinkles occur in many biological and physical systems. They have manifold technological applications, such as pressure sensors, functional coatings and diffraction gratings. In biology, substrates with an undulated surface promote the growth direction of cells or allow monitoring the stress a cell exerts on a substrate, e. g., during locomotion[1].
An everyday example of wrinkle formation is found in human skin. It consists of three layers: The epidermis forms the topmost layer with an extent of only 50–100 µm. Underneath it lies the dermis, with a layer thickness between 1 and 3 mm and the last layer is the hypodermis (layer thickness: 0.5–30 mm). During muscle contraction, the skin gets compressed and starts wrinkling[2,3]. With increasing age, the structure and mechanical properties of the skin change, which influences the appearance of occurring wrinkles. While they feature small wavelengths and amplitudes at young age, both these properties increase with advancing age and eventually, the wrinkles become visible. This is explained by the loss of elasticity of the skin[2,3].

The necessary requirement for the formation of wrinkles is a stress mismatch between the different layers[3–5]. Model systems, for example resembling human skin, were developed to study wrinkle formation. In these artificial systems, the thick elastic layer consists of a polymer, generally using polydimethylsiloxane (PDMS), while the thin solid cover layer is made of silicon dioxide[6] or metal[7]. Wrinkles are induced by heating the PDMS, coating it with the top layer, which is oxidized and then allowed to cool down[6].

The PDMS substrate can also be covered using thin polymeric film (i. e., liquid crystal elastomers), resulting in a system with temperature-dependent wrinkling[8].

Wrinkles have also been observed in bubbles with an elastic shell, made out of a protein, and deflated through a capillary. In these systems, they are formed from the basis of the capillary up to the equator of the bubble. In this case, wrinkling occurs when the molecules have reached their maximum packing density, which is directly connected with a finite positive surface tension[9,10]. However, most theoretical models assume a vanishing interfacial tension when buckling occurs, such that the deformation out of the plane costs only little surface energy[9].

Rupturing liquid films of high viscosity can also demonstrate wrinkling. Such films are dome-shaped viscous bubbles formed on a viscous fluid by inflating air at the bottom of the fluid container. The hemispherically shaped bubbles collapse and a hole emerges at their very top around which a rippling instability occurs. The number of ripples depends on the base radius of the bubble and is affected by the interplay between compression, gravity and bending[11,12]. These viscous bubbles form wrinkles because of a lateral compression. Such a compression can also be found in the system studied in this work.
Free-standing liquid crystalline films are an interesting system for studying undulations or other periodic structures of smectic layers. t is likely that elastic deformations of the molecular layers due to hydrodynamic causes can only be investigated in such systems or in microfluidic arrangements. This is due to the fact that they provide access to material properties that are not observable in thin cells, namely the coupling of forces and movements in the smectic layer plane to deformations of this plane, i. e., budding or wrinkling.

Smectic membranes that show surface wrinkling can act as a model system for biological cells, such as white blood cells or plant cells. Blood cells show wrinkling to gain excess membrane area when the cell needs to expand. Such an expansion is necessary due to osmotic swelling, or if the cell adheres to surfaces or scans them[13]. Plant cells need to respond to osmotic pressure by changing their surface and volume. Since the lipid membrane is inelastic, it expands or reduces its surface by exo- and endocytosis[14].
In this work, the formation of wrinkles and small protrusions of the bubble surface (so-called tubuli) on freely floating liquid crystalline (LC) bubbles are studied (Fig. 1). In contrast to soap bubbles, LC bubbles are stable over a much longer period, since they do not drain due to their internal layer structure. Additionally, the inner structure of the fluid allows us to observe these wrinkles. In soap films wrinkles cannot emerge, since a reduction of the film area only results in a thickening of the fluid layer, which is an instantaneous process.

The occurrence of wrinkles has been first reported in the work of K. Harth[15]. This work is continued here, now focusing on the dynamics of wrinkle formation. The bubbles are created by a collapsing catenoid-shaped LC film[16]. Two distinct scenarios in which wrinkles occur are found: compression by oscillating films and infolding of the bubble pole.

[a)]Electronic mail: patricia.pfeiffer@ovgu.de

Tubuli occur in general in regions of higher film thickness, (i. e., on an island) during the relaxation process from an elongated bubble towards a sphere.

Wrinkles observed on the smectic bubbles cannot be explained by the pure elasticity of the liquid crystal, as this would only lead to spreading, bending and/or twisting of the director field. This study investigates, whether wrinkling can be specifically generated by an external force or geometric boundary conditions, and whether internal processes of the liquid crystal membrane, for example, a rapid reduction of the film surface, can also lead to wrinkling.

II. MATERIAL AND METHODS

In all experiments, an achiral smectic C (at room temperature: 21 to 23 °C) LC is used, prepared from a 50/50 vol% mixture of 2-(4-n-Hexyloxyphenyl)-5-n-octylpyrimidine and 5-n-Decyl-2-(4-n-octyloxyphenyl)pyrimidine (Synthon Chemicals, Germany). Bubble preparation is carried out according to the method described in Ref.[17].

Fig.1 depicts the collapse of the catenoid schematically. The deflated bubble is formed as follows: The LC is placed between two circular supports (diameter: 5 cm) that are slowly pulled apart. After surpassing a certain distance ($D \gtrsim 1.32R$, R - radius of the circular supports[18]) of the rings, the intermediate catenoid LC film collapses and forms a satellite bubble[19]. Additionally, an oscillating remnant film remains in each support.

Different magnifications are used to either measure the oscillations of the remnant films in the catenoid supports (dashed box in Fig. 1(a) marks the imaged region for low magnification) or to resolve the wrinkles in detail.

Wrinkle formation is monitored with a Photron AX200 high-speed camera (at frame rates of 10,000 fps) from the side and illuminated with a high power LED with a wavelength of λ=530 nm(cf. Ref[17]).

Image analysis is carried out using MATLAB (version R2017b, The Mathworks Inc.). The wavelength of the wrinkles is determined using the two-dimensional spatial Fourier transform.

The two-dimensional fluid flow is characterized with an optical flow algorithm (see Refs.[20–22]) that combines a local approach, the Lucas-Kanade method, and a global one, the Horn-Schunck method. This results in a dense flow field that is robust against noise[22]. For this, it is assumed that the gradients of gray values (I - pixel intensity, x, y - spatial coordinates of the pixel, t - time) in an image do not change when being displaced, i. e.:

$$\nabla I(x,y,t) = \nabla I(x+u, y+v, t+1),$$

with the spatio-temporal gradient $\nabla = (\partial_x, \partial_y, t)^\top$[21]. To compensate for the ill-posedness of the problem, different smoothing techniques are applied within both parts (i.e. local and global) of the algorithm[22]. For a detailed description of the algorithm see Ref.[22].

In addition to the movement on the bubble surface, motion of the bubble itself takes place, too. This motion must be subtracted from the motion of the bubble surface. Therefore, the area of the bubble is detected and its centre of mass is calculated. The motion of the centre of mass is subtracted from each point of the velocity field of the entire frame, yielding a flow on the bubble, independent from its motion in the laboratory system. The results of the optical flow measurements are presented as colour-coded velocity maps (showing absolute velocity). Orange arrows are added to depict the direction of motion.

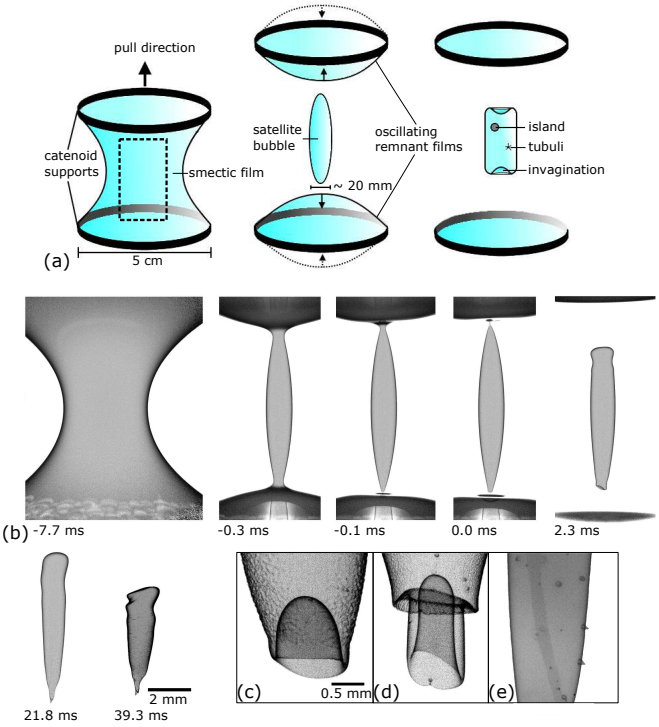

FIG. 1. (a) Sketch of the catenoid collapse, resulting in two films that remain in the catenoid supports and a small satellite bubble. This bubble can form invaginations at its poles, wrinkles and tubuli in regions of higher film thickness (i. e., islands). The dashed box (leftmost image) marks the imaged region. (b) Image sequence of a catenoid collapse and the evolution of the satellite bubble. The pinch-off of the bubble from the top and bottom part of the catenoid happens with a time delay of 1 ms. Time point 0 ms corresponds to the time at which the bubble is constricted on both sides. At 39.3 ms, the bubble has already formed some tubuli (small black dots) and wrinkles. (c) Detail image of randomly oriented wrinkles. (d) The bubble pole shows a double invagination and wrinkles. (e) Tubuli on a bubble. The darker regions are islands.

The film thickness of the elongated bubble is calculated after background subtraction from an average of several lines in the transmission images with the method described in Ref.[23]. Only the uniform (background) film is taken into account and island areas are excluded.

III. DYNAMICS OF WRINKLE FORMATION

The catenoid collapse and bubble pinch-off is illustrated schematically in Fig Fig. 1(a). For comparison, a time series of real data is given in Fig. 1(b). Time zero corresponds to the instant when the satellite bubble has fully detached (the pinch-off at the upper and the lower end occurs with a delay of 1 ms). Initially, the bubble has an elongated, hose-like shape (0–21.8 ms), until it relaxes towards a sphere. During the relaxation process, the bubble forms wrinkles at $t = 39.1$ ms as well as tubuli (black dots on the bubble). In Fig. 1(c), a detail image of randomly oriented wrinkles is depicted. Fig. (d) shows a double invagination scenario at the lower end of the satellite bubble and additional wrinkles formed above the infolded area. In (e), tubuli that grow on regions of higher film thickness are shown. They appear darker than the surrounding film.

Throughout all experiments, only two scenarios are found that lead to wrinkles on smectic LC bubbles. The first one shows wrinkles on an elongated bubble (Fig. 2).In the second scenario, wrinkling occurs immediately after the catenoid collapse, when the hose-like shaped bubble forms an invagination at the bottom end (Fig. 5). Next, both scenarios are discussed separately.

A. Compression leading to wrinkles

Wrinkles caused by compression occur on elongated bubbles. After the pinch-off of the bubble, typically remnant films remain in the catenoid supports. The oscillations of the films compress the elongated bubble along its length axis when both films move towards the bubble. This compression yields horizontally oriented wrinkles as shown in Figs. 2 and 6. The remnant films oscillate either in anti-phase when the pinch-off of the bubble occurs simultaneously at both ends or out-of-phase when a delayed pinch-off (typically around 1 ms) occurs. The oscillation frequency of the remnant films is 16 Hz for catenoid supports of 5 cm diameter.

Fig. 2 shows a typical time series of the compression of an elongated bubble. Horizontally oriented wrinkles are formed at $t = 34$ ms. The lower film reaches its closest distance to the bubble at $t = 44.5$ ms and the upper one at $t = 55.0$ ms, leading to a compression of the bubble. To reveal the flow on the bubble, an optical flow analysis is performed (see Fig. 2(b)). It becomes apparent that at time points $t = 37$ ms and 41 ms, a distinct upwards movement of the lower end of the bubble takes place with a velocity of about ≈ 0.3 m/s. This motion is caused on one hand by the relaxation of the bubble and on the other by the compression of the lower oscillating film.

To separate these two effects, the positions of the poles of several bubbles are followed over time. The results of one them are exemplary shown in Fig. 3(a). Since the pinch-off of both bubble poles happens simultaneously in this setting, the remnant films oscillate synchronously in anti-phase. The bubble is therefore compressed from both ends with the same velocity, which can be seen from the slopes of the green lines, which is $\approx 0.13 \pm 0.02$ m/s. In case the remnant films do not

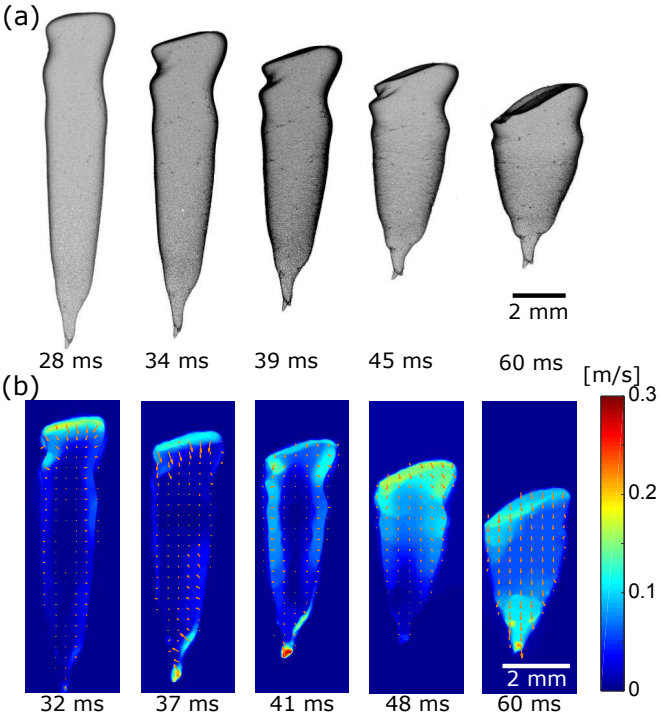

FIG. 2. (a) Image sequence of the formation of wrinkles due to the pressure of remnant films in the catenoid supports. Time zero corresponds to the pinch-off. The time points at which the remnant film reach their closest positions to the bubble are $t = 44.5$ ms and $t = 55$ ms after pinch-off for the lower and upper film, respectively. (b) Optical flow images of the compression of the bubble by the lower remnant film (comparison of two images with a time delay of 1.0 ms). The maximum flow occurs at the lower pole of the bubble at $t = 41$ ms caused by the lower remnant film. The flux caused by the upper film occurs at $t = 48$ ms.

oscillate synchronously, the bubble poles will move towards the bubble's centre of mass with different velocities. The contributions of relaxation of the bubble and compression can only be separated if the films do not oscillate in anti-phase, since the upper pole of the bubble would move downwards more slowly than the lower pole would move upwards. This means that the compression by the lower film shortens the bubble faster than it would shorten through pure relaxation. Once the bubble becomes shorter due to the relaxation process, the surface flow velocity approaches similar magnitude as found by measuring the bubble length.

The reduction of surface area of a wrinkled bubble is plotted in Fig. 3(b). The slope of the reduction rate changes with time. During region I it is $250 \pm 30\,\mathrm{mm}^2/\mathrm{s}$ and in region II it increases to $650 \pm 20\,\mathrm{mm}^2/\mathrm{s}$. Between $t = 25$ and $t = 55$ ms, both remnant films move towards the bubble and accelerate the rate of shrinkage. The volume of the bubble can be considered to remain constant.

These values for the rate of surface reduction can be confirmed assuming a cylinder of constant cross-section and time-varying height during the time interval $t \in [25,55]$ ms (i. e., the time when the lower film moves towards the bubble). Considering the elongated bubble as a cylinder (which is reason-

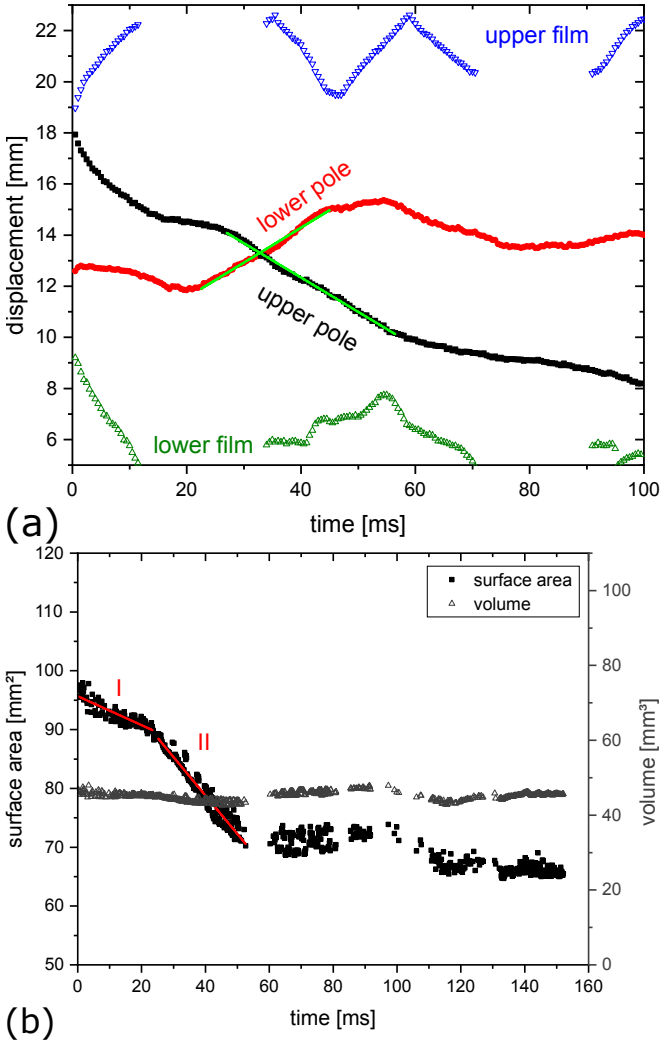

FIG. 3. (a) Positions of the bubble poles over time (top and bottom; filled symbols) due to surface reduction and bubble compression. The open triangles denote the position of the remnant film in the upper (▽) and lower (△) film holder over time. The green lines mark the slope of the position of the bubble poles, which is 0.13±0.02 m/s for the lower pole and 0.14±0.02 m/s for the upper one. (b) Surface reduction and volume of a relaxing bubble ($t = 0$ ms corresponds to the bubble pinch-off). The surface reduction rate between in the first segment is 250±20 mm^2/s and in the second it increases to 650±30 mm^2/s. The volume is an indicator for the reliability of the data, since it is assumed to remain constant during relaxation.

able at this early state of relaxation; cf. Fig. 2), the surface area reduction due to decreasing height and increasing radius of the cylinder can be estimated to be 400±200 mm^2/s. This value is comparable to the surface reduction rate calculated from the accurately estimated surface reduction, which is 250±20 mm^2/s. After $t = 25$ ms (the bubble still has a hose-like shape), the surface reduction rate determined by the height of a cylinder increases to 1000±50 mm^2/s, which is also comparable to the value estimated from Fig. 3(b)). The significant difference in the surface reduction rate in region I and II of Fig. 3(b) can only be attributed to the compression caused by the remnant films.

From the acceleration of the remnant film towards the bubble, the force acting on the bubble can be calculated. It lies around 10^{-5} N with an acceleration of 0.45 m/s^2. With a diameter of the oscillating film of 5 cm, the pressure acting on the bubble lies around 10^{-3} N/m^2, which decays with increasing distance between film and bubble.

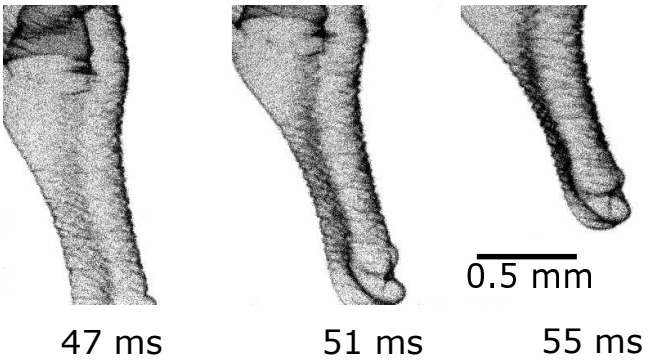

FIG. 4. Visible profile of wrinkles on a bubble tail in detail at different time points. The tail shortens over time and the wrinkles become more pronounced.

In a detail view, the profile of the wrinkles can be observed (Fig. 4). This provides access to the amplitude a of the wrinkles, which is $10 \pm 2\,\mu$m. The time series of the wrinkles shows that the bubble tail becomes shorter with time. However, the wavelength of the wrinkles increases. This means that the total surface area of the bubble remains constant. This is also confirmed by the following: Comparing the length of the bubble tail between 47 and 55 ms, the length of the bubbles decreases by 25%. Let us approximate the bubble tail by an one-dimensional line whose length increases by a sinusoidal undulation (cf. Fig. 4). The length S of the curve can be calculated than as:

$$S = \int_0^L \sqrt{1 + \frac{4\pi^2 a^2}{\lambda^2} \cos^2\left(\frac{2\pi x}{\lambda}\right)}\,\mathrm{d}x,$$

Taking a wrinkle wavelength of $\lambda = 50\,\mu$m and an amplitude $a = 10\,\mu$m as at t=47 ms, with the length L of 17 periods within 0.9 mm length. Thus, $S \approx 1.25$ mm due to sinusoidal wrinkling. Calculating now the length of the bubble at t=55 ms ($\lambda = 57\,\mu$m and $a = 22\,\mu$m, $L = 12$ periods within 0.5 mm length), then S=1.24 mm. This shows that the overall surface of the bubble remains constant, however, the local surface per area unit increases and with it the local surface energy with the same rate.

B. Wrinkles caused by invagination

The second scenario in which wrinkling occurs is the invagination of the bubble at its lower pole (Fig. 5(a)). After pinch-off at the bottom part ($t = 0.3$ ms), the bubble forms a

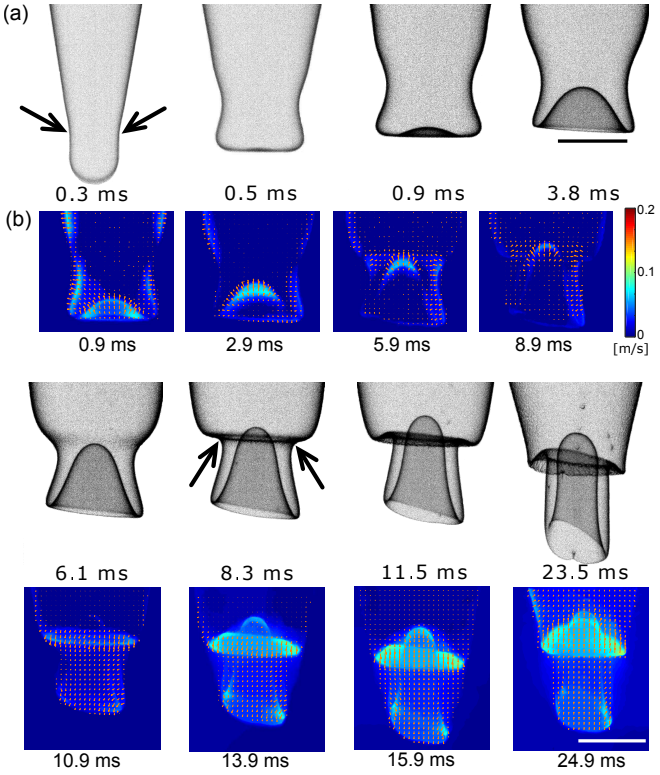

FIG. 5. (a) Image sequence of the formation of wrinkles due to invagination of the bubble after pinch-off ($t = 0$). (b) Optical flow images of the invagination of the bubble (comparison of two images with a time delay of 1.0 ms). The smectic material flows mainly into the disc-shaped area. Scale bar: 1 mm.

small undulation (arrows), which can be identified as a capillary wave originating from the pinch-off at the lower pole. The wave travels upwards along the bubble and becomes more pronounced. The velocity of the wave propagation decreases with time. In addition to this traveling undulation, the bubble forms an invagination at its very end (here at $t = 0.9$ ms) that also propagates upwards, too, but much faster than the undulation itself (which slows down over time). When the top end of the invagination comes close to the vertical position of the undulation, the film forms a second invagination (arrows at $t = 8.3$ ms). This causes the onset of wrinkling, which is already visible in the disc-shaped area around the invagination (cf. central region at $t = 11.5$ ms in Fig. 5(a)).

Some LC material flows into this second invagination, which is depicted in the optical flow images by the orange arrows, see Fig. 5(b). Here, the direction of the flow changes at $t = 8.9$ ms from an upwards stream in the invagination to a stream pointing downwards at $t = 10.9$ ms in the disc-shaped area around the invagination. The material that is floating here originates from the upper part of the bubble and is collected in this disc-shaped area. As a consequence of the bubble tail becoming elongated further, a downwards stream below the disc-shaped area is also present. Additionally, the conical shape of the bubble leads to a decreasing film area with a decreasing distance to the bubble poles. In other words, when the invagination collects film material from above, where the circumference of the bubble is larger than at its poles, the available area for the film material decreases rapidly. Besides that, the lower pole shrinks in size close to the area of invagination. At $t = 24.9$ ms, a motion of the conical bubble area towards the centre of the bubble can be seen, which is causing the onset of wrinkling. It can be noted that at that time, the flow rates have different magnitudes (see arrows), which is likely to be responsible for a light asymmetry of wrinkles (i. e., the wrinkles are more pronounced at the left side).

The area reduction triggered by the double-invagination scenario yields a pronounced appearance of wrinkles. They have no preferred orientation, since the film is compressed from all directions. Due to the complicated invagination of the bubble, it takes a long time to unfold and hence, to reach spherical shape (i. e., around 150 ms). During the unfolding process, the bubble forms new smectic layers (i. e., islands)[17] mainly in the regions without wrinkles. In these regions, the material to form new layers can only originate from the surface shrinkage of the bubble. However, the surface in the wrinkled region must reduce quickly when the wrinkles disappear, such that it can be assumed that a flow of smectic material away from the wrinkled regime takes place and aggregates on the already existing islands.

C. Wavelength of Wrinkles

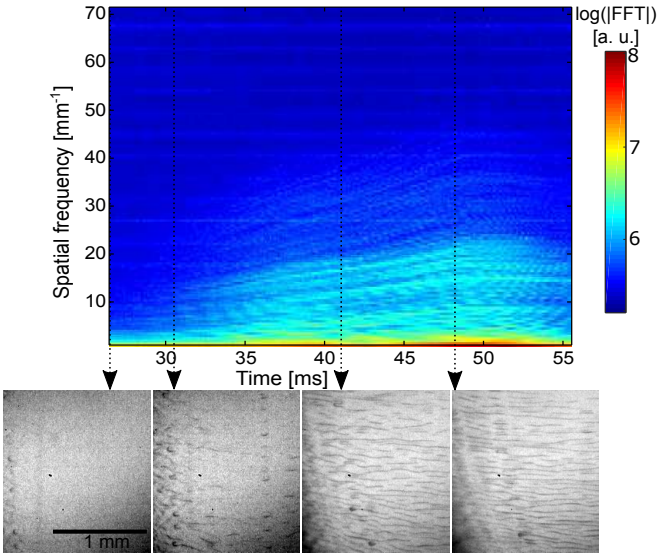

FIG. 6. Spectrogram of the wrinkles. The change of the wavelength of the wrinkles over time is depicted with the corresponding snapshots of the bubble. The colour indicates the absolute value of the Fourier transform. The wrinkles occur gradually and over time their wavelength decreases from approx. 55 µm at $t = 41$ ms to 45 µm at $t = 48$ ms. Spatial resolution: 7 µm/pixel.

The wavelength and orientation of the wrinkles can be determined from the amplitude spectrum of the spatial Fourier transform. Typical values for the wavelength lie between 20 and 70 µm. Fig. 6 shows a spectrogram of the wrinkles with the corresponding snapshots of the experiment. The wrinkles

are horizontally arranged and the wrinkle wavelength changes from around 55 µm at $t = 41$ ms to 45 µm at $t = 48$ ms. This is caused by the oscillations of the remnant films, which compress the bubble along its length axis. In many cases, the remnant films show different modes, such that they do not move straight towards the bubble ((0,1) mode), but show an oscillation in the (1,1) mode. Thus, the compression of the bubble is time dependent and hence, the wrinkle wavelength.

D. Tubuli formation

Tubuli are small protrusions on the smectic film, which often appear during bubble relaxation. Their occurrence was previously reported in Refs.[15,16,24,25]. These structures are formed in regimes of higher film thickness (i. e., on islands) as shown in Fig. 7. A typical diameter of these islands is 0.2 mm. The protrusions themselves are smaller, featuring diameters in the range of 10 to 90 µm. The diameter of the protrusions decreases slightly after formation, whereas their length increases, as if they were stretched. If their diameter becomes too small (i. e., shorter than ≈90 µm), the tubuli will pinch-off from the mother bubble.

Tubuli can occur in addition to wrinkles (dark spots in Fig. 5(d)). The formation of wrinkles and islands does not depend on each other. TTubuli, which are generated on islands can occur without the formation of wrinkles and the other way around. If they occur together with wrinkles, they are generated prior to wrinkling. However, wrinkles can form around tubuli and arrange perpendicularly to the latter, such that they are organized in a star-like manner around the tubuli. The wavelength of these wrinkles remains constant. The relaxation dynamics of the wrinkles around tubuli is as follows: In the direct vicinity of the tubuli (i. e., 30 µm), the wrinkles disappear very slowly during the bubble relaxation. They exist almost as long as the tubili themselves. At larger distances, such wrinkles disappear as fast as wrinkles that are not located around tubuli.

During bubble relaxation, the surface area of the smectic bubble decreases. As a result, islands grow, since they collect the excess material. Islands on which protrusions are formed also grow in size. In Fig. 7, the diameter of the right island in the black circle grows from 0.14 mm at t=24.5 ms to 0.21 mm at t=40.5 ms.

Tubuli can be located on each spot on the bubble; even on invaginated sections. However, they are mainly directed towards the outside of the bubble. Only in rare cases they are found to point inwards (arrow in Fig. 7).

IV. DISCUSSION

The study of wrinkles in LC bubbles reveals a clear picture of their formation. While in elastic sheets or membranes, an elastic instability causes wrinkles – i. e., an in-plane compression results in a deformation out of the plane – wrinkling in LC membranes is caused by an external force. Two different mechanisms causing wrinkles are identified: A lateral compression of the bubble and invagination of its lower pole. The lateral compression is caused by two remnant films, which remain in the catenoid holders. This is visible in the surface reduction process of the bubble (cf. Fig. 3(b)), where two different shrinking rates are found. The first one is caused by the surface reduction rate of the bubble due to reorganization of the smectic material and the second one is mainly caused by compression of the oscillating films. However, the overall surface of the bubble remains constant, only the local surface per area unit increases. Thus, the two different shrinking rates are an artifact of the measurement caused by the limited spatial resolution taken for the surface determination. The method does not take the wrinkled surface into account, but only the shape of the bubble.

The positions of the bubble poles in the shown example (Fig. 3(a)) change with the same ratio. This is caused by the anti-phase oscillations of the remnant films. However, the bubble only shows wrinkles at the lower end, which can be explained by the shape of the bubble itself. The upper pole typically becomes round, with a mushroom-like shape at the top and a conical shape at the bottom pole. Thus, the film area at the latter decreases with a decreasing distance to the bubble pole. Due to the compression from the oscillation of the remnant film, the length of the bubble additionally decreases. These differences in shape between the upper and lower pole of the bubble might be caused by gravity and are responsible for the occurrence of the wrinkles mainly at the lower pole of the bubble. However, not all experiments reveal these two regimes of surface reduction (cf. Ref.[17]). This may have various reasons: First of all, the distance between bubble and remnant films plays an important role, since the pressure acting on the bubble decreases with the distance. Thus, it has largest effect on the bubble shortly after pinch-off and if the bubbles adopts its equilibrium shape quickly, the oscillations are not fast enough to act on the bubble. Another reason is that the upper catenoid support continues moving upwards after the catenoid collapse and must be stopped by hand. This results in a larger distance between upper film and bubble than between lower film and bubble. Hence, the bubble compression from above becomes weaker with time. In some cases, the films in the catenoid supports rupture and the bubble is not affected by their oscillations at all.

Another scenario yielding the formation of wrinkles is the double invagination of the bubble at its lower pole (Fig. 5). Here, the onset of wrinkling is caused by the decreasing surface area at the lower bubble pole (excluding the invagination itself). In fact, only the area around the second invagination and above shows the surface deformation. The tail (i. e., the area between the pole and the second invagination) is free of wrinkles. In this region, the surface area increases significantly, instead. However, it is not obvious, where the material comes from. One explanation could be that the material comes from additional smectic layers (i. e., islands), which are present in the majority of experiments. Another source might be the material that runs into the disc-shaped area around the invagination. A downward flux, originating from the disc-shaped area is observed in the optical flow images.

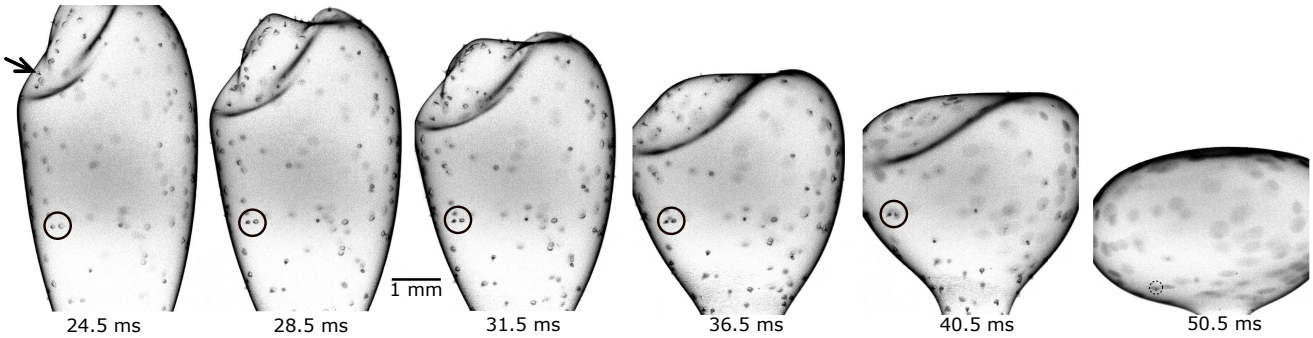

FIG. 7. Image sequence of developing tubuli on a bubble. Tubuli form at those positions where the film possess islands, i. e., areas with a larger film thickness. The black circle marks the same pair of islands in each image. Out of these islands, tubuli are formed, whose diameters decrease and lengths increase with time. Tubuli can also pinch-off from the main bubble, as the one in the dotted circle. The arrow at $t = 24.5$ ms points on a protrusion, which points into the bubble.

In general, wrinkle formation in smectic LC films is only possible when the lateral compression of the bubble is much faster than smectic layer formation, since the local surface energy of the bubble increases.

The pressure acting on the bubble produced by oscillating remnant films affects the bubble within 30 ms (oscillation frequency 16 Hz). This time is typically needed for the bubble to form wrinkles of a certain wavelength. This value can also be achieved by calculating the growth time scale of buckling: $\tau = d/(2\gamma v_0)$[26], with d the diameter of the bubble, v_0 the impact velocity, and γ the grade of reflection of the compression front at the opposite end of the material ($\gamma = 1$ – no reflections, $\gamma = 2$ – one reflection). For a typical elongated bubble ($d = 2$ mm, $v_0 = 0.4\,\mathrm{m\,s^{-1}}$, $\gamma = 1$) this yields $\tau = 2.4 \pm 0.4$ ms, which agrees perfectly with the value determined from the high-speed videos. From this, it can be assumed that the liquid crystal material behaves similarly to a solid on short time scales (i.e., a few milliseconds). From the time scale of wrinkle formation and the surface reduction rate of the bubble (which lies around 40 ms[17]), it can be estimated that the time scale of the formation of new smectic layers lies below 10 ms. This is longer than the time the pressure produced by oscillating remnant films is acting on the bubble, and and one order of magnitude smaller than the relaxation time. Bubbles with a film thickness below 16 nm do not show wrinkling. They relax rapidly towards a sphere (within 10 ms, cf. Ref.[17]) and the oscillations of the remnant films are to slow to act on the bubble. The formation of wrinkles on LC films was reported only recently[25]. The authors identified the same scenarios of wrinkle formation and developed a model for their description. In the work presented here, a detailed analysis of the flow on the bubble is provided.

Membranes in a fluid environment affected by external forces show buckling as well. The time scale of their evolution depends on the fluid viscosity and the wavelength of the developing buckles[27]. In the experiments, those two parameters will also be important, however, the thickness of the liquid crystal film is another crucial value. Additionally, the applied stress on a membrane or LC film must act long enough that buckling becomes visible[27].

The local surface area also increases during formation of tubuli, which is energetically unfavourable for the system. They are growing out of regions of higher film thickness (islands). The material for their formation must be collected from the surrounding film, since the islands are still growing in size despite the tubuli formation. The question remains why the islands form protrusions instead of simply grow faster. It can be assumed that the line tension of the island plays a crucial role here: The line tension keeps the circumference of the islands as short as possible due to energy minimization. Thus, there might be a competition between the line tension of the island, which prevents the island from growing as fast as possible, and the amount of material that runs into the islands due to the decreasing surface area of the bubble. The fact that tubuli can occur without surface wrinkling underlines this assumption and is consistent with what has been reported in Refs.[24,25]. The authors suggested that the formation of tubuli occurs due to a fast surface reduction of the bubble (too fast for the formation of new smectic layers) and probably, the smectic film behaves on short time scales (i. e., within a few milliseconds) like a structure with zero effective surface tension. In such a setting, a critical thickness of islands that form tubuli could not be assumed.

V. CONCLUSIONS

In this study, wrinkle formation on thin LC films is investigated, namely the formation of wrinkles. This phenomenon cannot be found in experiments in LC sandwich cells.

Two scenarios are found in which wrinkling occurs: compression due to the oscillations of remnant films in the catenoid supports and double invagination of the bubble at its lower pole shortly after pinch-off. Which of the cases occurs depends on the kind of stress on the bubble surface.

Compression of the elongated bubble along its length axis is caused by remnant films that remain in the catenoid supports. As a result, horizontally oriented wrinkles are formed. The double invagination occurs due to a small undulation and an invagination at the lower pole of the bubble. When the invagination reaches the height of the undulation, the bubble forms a second invagination at this position and the film above

starts wrinkling as a result of a compression from all directions, since the circumference of the bubble decreases. The wavelength of the wrinkles is governed on one hand by the film thickness and on the other hand on the stress applied to the bubble. Wrinkle formation occurs as a response to an outer force that acts faster on the film, than the smectic material is able to form new layers to reduce its surface area. The experimental data provide an adequate access to the dynamics of the reorganization process of smectic layers.

Furthermore, the formation of small protrusions of the smectic film is studied, which occur on thicker regions of they film (i. e., on islands) due to a competition between the line tension of the islands and the amount of excess material (which is produced by surface reduction of the bubble) accumulating at the islands.

In future experiments, the effect of viscosity, geometric confinement and film thickness on wrinkle formation will be studied. The role of film thickness must be studied over a larger order of magnitude, to evaluate the dependency between film thickness and wavelength. The preparation of thicker films is a necessary step to fully understand the system. However, this can only be realized using other smectic LCs that would have different physical properties (e. g. viscosity or elasticity), making a comparison between the results challenging.
Another interesting aspect would be to increase the forces on the bubble. Instead of the oscillating remnant films, ultrasound transducers could be used. However, the bottleneck is the destruction of the smectic films. It is only possible to puncture them, while the films move away from the bubble. This might be already be to late to observe a significant effect. As far as tubuli formation is concerned, the role of the line tension of islands must be identified, when the film shrinks. For this purpose, again, the production of thicker smectic bubbles is needed, to study the effect of slower surface reduction rates on the formation of tubuli.

ACKNOWLEDGMENTS

The Deutsche Forschungsgemeinschaft, DFG, is acknowledged for support within projects STA 425/28-2 and DA 2108/1-1. The research was started in the lab of Ralf Stannarius, who is acknowledged for giving me the opportunity to learn from him.

[1] Harris, A. K., Wild, P., and Stopak, D. *Science* **208**(4440), 177–179 (1980).
[2] Serup, J., Jemec, G. B. E., and Grove, G. L. *Handbook of non-invasive methods and the skin*. CRC press, (1995).
[3] Genzer, J. and Groenewold, J. *Soft Matter* **2**, 310–323 (2006).
[4] Pocivavsek, L., Dellsy, R., Kern, A., Johnson, S., Lin, B., Lee, K. Y. C., and Cerda, E. *Science* **320**(5878), 912–916 (2008).
[5] Tokudome, Y., Suzuki, K., Kitanaga, T., and Takahashi, M. *Sci. Rep.* **2**, 683 (2012).
[6] Bowden, N., Huck, W. T. S., Paul, K. E., and Whitesides, G. M. *Appl. Phys. Lett.* **75**(17), 2557–2559 (1999).
[7] Bowden, N., Brittain, S., Evans, A. G., Hutchinson, J. W., and Whitesides, G. M. *Nature* **393**(6681), 146–149 (1998).
[8] Agrawal, A., Luchette, P., Palffy-Muhoray, P., Biswal, S. L., Chapman, W. G., and Verduzco, R. *Soft Matter* **8**, 7138–7142 (2012).
[9] Aumaitre, E., Knoche, S., Cicuta, P., and Vella, D. *Eur. Phys. J. E* **36**(3), 22 (2013).
[10] Knoche, S., Vella, D., Aumaitre, E., Degen, P., Rehage, H., Cicuta, P., and Kierfeld, J. *Langmuir* **29**(40), 12463–12471 (2013).
[11] Debrégeas, G., de Gennes, P.-G., and Brochard-Wyart, F. *Science* **279**(5357), 1704–1707 (1998).
[12] da Silveira, R., Chaïeb, S., and Mahadevan, L. *Science* **287**(5457), 1468–1471 (2000).
[13] Wang, L., Castro, C. E., and Boyce, M. C. *Soft Matter* **7**, 11319–11324 (2011).
[14] Staykova, M., Holmes, D. P., Read, C., and Stone, H. A. *Proc. Nat. Acad. Sci. USA* **108**(22), 9084–9088 (2011).
[15] Harth, K. *Episodes of the Life and Death of Thin Fluid Membranes*. PhD thesis, Otto-von-Guericke-Universität Magdeburg, (2016).
[16] May, K., Harth, K., Trittel, T., and Stannarius, R. *Europhys. Lett.* **100**, 16003 (2012).
[17] Dähmlow, P., Trittel, T., May, K., Harth, K., and Stannarius, R. *Liq. Cryst.* **45**(7), 993–1003 (2018).
[18] Amar, M. B., da Silva, P. P., Limodin, N., Langlois, A., Brazovskaia, M., Even, C., Chikina, I. V., and Pierański, P. *Eur. Phys. J. B* **3**, 197–202 (1998).
[19] Müller, F. and Stannarius, R. *Europhys. Lett.* **76**(6), 1102–1108 (2006).
[20] Liu, C. *Beyond Pixels: Exploring New Representations and Applications for Motion Analysis*. PhD thesis, Massachusetts Institute of Technology, (2009).
[21] Brox, T., Bruhn, A., Papenberg, N., and Weickert, J. In *Computer Vision - ECCV 2004,* Pajdla, T. and Matas, J., editors, 25–36 (Springer Berlin Heidelberg, Berlin, Heidelberg, 2004).
[22] Bruhn, A., Weickert, J., and Schnörr, C. *Int. J. Comput. Vis.* **61**(3), 211–231 (2005).
[23] Stannarius, R., Cramer, C., and Schüring, H. *Mol. Cryst. Liq. Cryst.* **329**(1), 423–431 (1999).
[24] May, K., Harth, K., Trittel, T., and Stannarius, R. *ChemPhysChem* **15**, 1508–1518 (2014).
[25] Harth, K., Trittel, T., May, K., and Stannarius, R. *Soft Matter* (2019).
[26] Gladden, J. R., Handzy, N. Z., Belmonte, A., and Villermaux, E. *Phys. Rev. Lett.* **94**, 035503 (2005).
[27] Luo, H. and Pozrikidis, C. *Int. J. Solids Struct.* **44**(24), 8074 – 8085 (2007).